ADVANCED MATERIALS INTERFACES
Open Access
www.advmatinterfaces.de

Enhancing Penetration Performance and Drug Delivery of Polymeric Microneedles Using Silica Nanoparticle Coatings

Sohyun Kim, Hyewon Choi, Hyejoong Jeong, Wilfredo Méndez Ortiz, Hwayeong Cheon, Jae Yong Jeon, Jae Hyeon Lee, Jeong Hwan Han, Kathleen J. Stebe, Daeyeon Lee, and Hyunsik Yoon**

Microneedle (MN) technology offers a powerful approach for transdermal delivery enabling painless injection and facilitating self-administration without the need for professional assistance. However, the weak mechanical strength of MNs can lead to inefficient drug delivery and serious skin irritation if the MNs fracture during administration and leave fragments under the skin. Thus, the MNs need to be mechanically robust to avoid fracture during penetration through the skin while maintaining efficient drug delivery. Herein, the polymer-based MNs with layer-by-layer (LbL) films of silica (SiO_2) nanoparticles (NPs) and a polycation (poly(diallyldimethylammonium chloride) (PDADMAC)) followed by hydrothermal calcination are reinforced. The mechanical strength of the MNs is significantly improved after LbL assembly and shows lower threshold pressure to penetrate skins. Moreover, their drug loading and releasing properties are significantly enhanced due to an increase in the surface area and interfacial interaction. These SiO_2 nanoparticle-containing LbL thin films have great potential for the surface modification of 3D microstructured devices such as MNs, as evidenced by their enhanced mechanical strength and drug coating efficiency that result in a promising MN drug delivery model.

1. Introduction

Microneedles (MNs) have emerged as an attractive platform to enable interstitial fluid extraction and painless drug delivery.[1,2] MNs are actively being explored for drug delivery to treat various diseases and conditions, such as tumors, cancer, cardiovascular diseases and infectious diseases.[3–7] Additionally, MN-based sensors have gained tremendous attention for real-time diagnosis and wearable devices.[8–10]Various factors need to be considered to ensure successful insertion of the MNs into the skin, such as the material, needle geometries (e.g., height, diameter, tip diameter), and density.[11,12] In particular, the material that is used for MN fabrication determines many physical properties that are important for successful transdermal delivery of drugs.

Recently, polymers have been widely used to fabricate MNs because of their cost-effectiveness and ease of processing.[13–15] However, they have a relatively low Young's modulus compared to traditional materials that have been used for MN fabrication, such as glass, silicon, and metals. Additionally, MNs made with biocompatible polymers, such as poly(ethylene glycol) diacrylate (PEGDA), can swell when they are exposed to water or high humidity, further lowering their stiffness. Because materials with low Young's moduli tend to be flexible, MNs made with a low Young's modulus material may bend or buckle upon contact with the skin, negatively affecting their skin penetration.

S. Kim, H. Yoon
Department of Nano Bio Engineering
Seoul National University of Science and Technology
Seoul 01811, South Korea
E-mail: hsyoon@seoultech.ac.kr

H. Choi, H. Yoon
Department of Chemical and Biomolecular Engineering
Seoul National University of Science and Technology
Seoul 01811, South Korea

H. Jeong, W. M. Ortiz, K. J. Stebe, D. Lee
Department of Chemical and Biomolecular Engineering
University of Pennsylvania
Philadelphia PA 19104, USA
E-mail: daeyeon@seas.upenn.edu

H. Cheon, J. Y. Jeon
Department of Rehabilitation Medicine
Asan Medical Center
University of Ulsan College of Medicine
Seoul 05505, South Korea

J. H. Lee, J. H. Han
Department of Materials Science and Engineering
Seoul National University of Science and Technology
Seoul 01811, South Korea

The ORCID identification number(s) for the author(s) of this article can be found under https://doi.org/10.1002/admi.202400212

DOI: 10.1002/admi.202400212

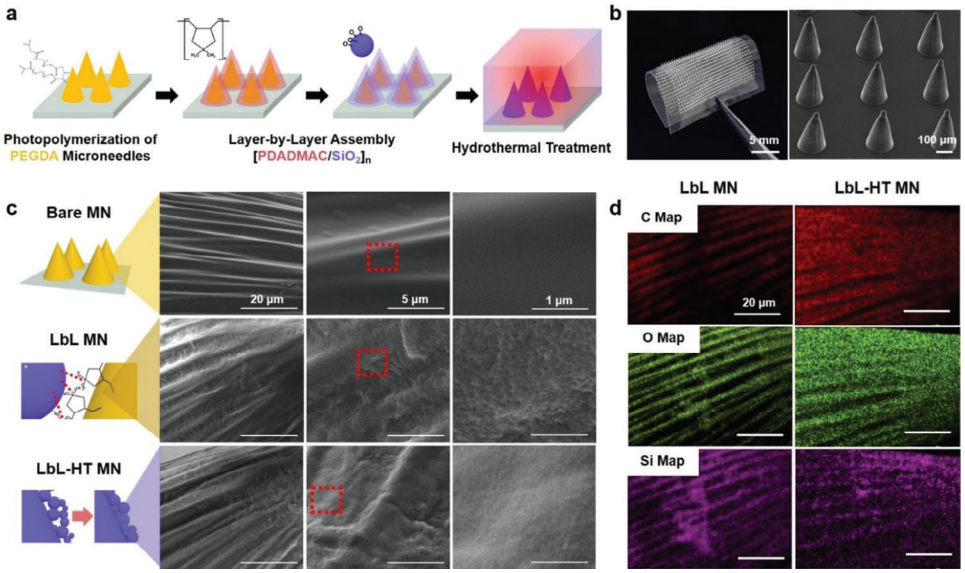

Figure 1. Preparation and characterization of the MNs. a) Schematic images showing three-step preparation: photopolymerization, LbL assembly, and hydrothermal treatment. b) Images of the fabricated MNs. c) SEM images of the MNs showing their surface morphologies. d) SEM–EDS mapping of each element showing the distributions of C, O, and Si atoms on the LbL and LbL-HT MNs.

Such a phenomenon reduces the effectiveness of MNs in achieving the intended drug delivery or sample collection. Therefore, in the design of MNs, a balance between the toughness and stiffness of the material is needed. MNs should be rigid enough to penetrate the skin while being sufficiently tough to minimize the risk of fracturing and causing associated pain or discomfort to the patient.[14] Identifying a single material that can meet all the requirements for effective transdermal delivery using MNs can, thus, be challenging.

Here, we show that MNs made of PEGDA could be mechanically reinforced, and thus, their dermal delivery could be enhanced by coating these MNs with layer-by-layer (LbL) films containing silica (SiO_2) nanoparticles (NPs). The LbL assembly method enabled the precise control over the thickness and composition of the coating without significantly altering the geometry of the MNs. Positively charged poly(diallyldimethylammonium chloride) (PDADMAC) and negatively charged SiO_2 NPs were alternatively deposited on the surface of photopolymerized PEGDA MNs. The LbL-modified MNs were hydrothermally treated to induce sintering between SiO_2 NPs. After the treatment, we coat colored dyes on the MNs and investigate their release behavior from the surface. In addition, we conduct mechanical tests and compare the pressure threshold for skin penetration using porcine skins and live animals. Our results show that LbL assembly followed by the hydrothermal treatment is an effective reinforcement method to enhance skin penetration, and in turn, resulting drug loading and release properties.

2. Result and Discussion

Figure 1a illustrates the three steps to produce SiO_2 NP-reinforced MNs via LbL assembly and a subsequent hydrothermal process. In a previous study, we fabricated PEGDA-based MNs via photolithography.[16] The fabricated MNs (width = 150 μm, height = 350 μm), as shown in Figure 1b, were exposed to UV to complete curing and pretreated with oxygen plasma to generate surface charge for LbL assembly. Since the MN surface was negatively charged via oxygen plasma treatment, the MN patches were first dipped in the cationic PDADMAC solution. Subsequently, the positively charged MN samples were dipped in the negatively charged SiO_2 NP suspension, followed by three rinsing steps. This sequential deposition of PDADMAC and SiO_2 NPs was repeated to acquire a thin film of a desired thickness. After finishing LbL assembly, the samples were placed in an autoclave for hydrothermal treatment. Hydrothermal treatment of SiO_2 NP-containing LbL films has been shown to dramatically enhance their mechanical durability.[17] Similar to Ostwald ripening, particles with smaller sizes dissolve owing to their high solubility and then precipitate in the high-curvature region to form these necks between contacting NPs under hydrothermal conditions.[17–19] Compared to thermal sintering, which requires a high temperature over 400 °C to achieve sintering between SiO_2 NPs, the temperature needed for hydrothermal treatment is moderate (123 °C) which enables mechanical reinforcement of SiO_2 NP-containing films on supports that have a low degradation temperature, such as polymers.

SEM images of the unmodified MNs (bare MNs), LbL-modified MNs (LbL MNs), and hydrothermally treated MNs (LbL-HT MNs) are shown in Figure 1c. After the preparation of samples by photolithography, MNs had wrinkles on their surfaces due to volume shrinkage.[20,21] The unmodified MNs did not show nanoscale features on their surfaces, whereas the LbL MNs and LbL-HT MNs showed nanoscale surface roughness, indicating the NP coating on the surface of the MNs. The surface of LbL MNs had spherical NPs, whereas the LbL-HT MNs showed a smoother surface, confirming the sintering of the SiO_2 NPs. The elemental composition of the outer surface of the thin films on the MNs, analyzed by energy dispersive X-ray spectroscopy (EDS), showed that SiO_2 NP coatings were uniform on the MN surfaces as shown in Figure 1d.

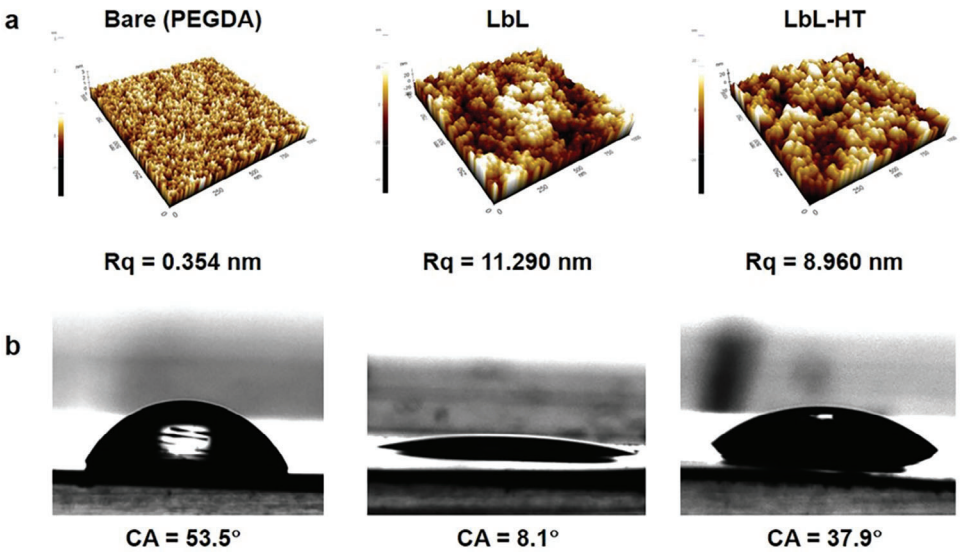

Figure 2. Surface roughness and hydrophilicity of the MNs. a) AFM images showing the surface morphology and roughness values of the bare, LbL and LbL-HT surfaces. b) Water contact angles of the bare, LbL and LbL-HT surfaces.

Figure 2a shows atomic force microscopy (AFM) images of the surfaces of the polymerized PEGDA, LbL and LbL-HT films. The bare PEGDA surface showed a roughness (R_q) value of 0.35 nm, which correlated to a smooth surface. The LbL-coated surface showed an R_q value of 11.29 nm, which is much higher than that of the bare surface due to the presence of SiO_2 NPs on the MN surface. The hydrothermally treated LbL surface showed a slightly lower R_q value of 8.96 nm; this showed the sintering effect of the silica nanoparticles after the hydrothermal process. Additionally, the presence of silica NPs caused a more hydrophilic MN surface, as shown in Figure 2b. Bare PEGDA MNs, which were not coated with SiO_2 NPs, showed a water contact angle of 53.5°, while the water contact angle of the LbL MNs decreased to 8.1° and 37.9°. The decrease in contact angle after the LbL process, a sign of increased hydrophilicity, can be attributed to the increase in the surface area and the presence of interconnected nanopores. The increase in contact angles after hydrothermal treatment could be explained by the reduction in the surface area and the porosity.

To characterize the drug delivery capability of the three types of MN patches, we used a dye as a model compound to evaluate their loading and release profiles, as shown in **Figure** 3a. First, we dipped the MN samples in the dye solutions for a specific period of time. Subsequently, the dye was released from the MNs into the phosphate-buffered saline (PBS) solution for an hour. Sulforhodamine B (SRB), a cationic dye, was used to observe the dye loading on the MNs because it is a widely used fluorescent dye as a drug model.[22] Figure 3b shows the images of the SRB-loaded MNs. Compared to that on the bare MNs, the dye loading on the LbL MNs and LbL-HT MNs was more uniform throughout the MN patches.

We also calculated the dye loading capacity for each MN using:

$$\text{Normalized dye } \textit{coating} \text{ capacity} = \frac{M_{\text{coated}}}{M_{\text{bare}}} \quad (1)$$

where M_{bare} (g) and M_{coated} (g) are the mass of the dye loaded on the bare MNs, and on LbL MNs and LbL-HT MNs, respectively. To compare the loading capacity, mass increases of MN patches after loading SRB for 0.5, 1, 4, and 8 h were measured by gravimetrically. Figure 3c shows a graph indicating an increase in dye loading as the dipping time was increased. The drug loading contents continuously increased for up to an hour, at which point the loading became saturated. The LbL-HT MN patch showed a 2.6-fold increase in dye loading capacity compared to bare MN. The LbL MN patch showed a 3.0-fold increase in dye loading capacity. These results showed that the increased cationic dye loading in LbL MN and LbL-HT MN patches was likely due to the increase in electrostatic interaction and surface areas due to the presence of SiO_2 NPs, as shown in Figure 2.

We also investigated the drug release properties of the dye-loaded MNs, as shown in Figure 3d. SRB were loaded onto the MNs for an hour and then released in the PBS solution (pH 7.4) for an hour. The LbL MNs and LbL-HT MNs exhibited higher release amounts than the bare MNs because the loading capacity was much higher with LbL and LbL HT MNs, as shown in Figure 3c. Interestingly, LbL-HT MNs showed the highest release value, although the loading capacity was not the highest (Figure 3d). The higher release amount of LbL-HT MNs compared to that of LbL MNs could be due to the loss of negative charge on in the LbL assembly, weakening the interactions between SRB and the coating, after SiO_2 NPs were sintered.

To assess the impact of these coatings on mechanical robustness of MNs, we conduct mechanical tests on MNs after LbL assembly and hydrothermal treatment. Such mechanical tests have been used for evaluating the mechanical robustness of features or roughnesses with high aspect ratio.[23] Because MNs have a high aspect ratio (above 2 in this study), MNs can be fragile when shear stress is applied. **Figure** 4a,b are an illustration and an image of the experimental setup for the mechanical test, respectively. The MN patches were placed on sandpaper and dragged horizontally

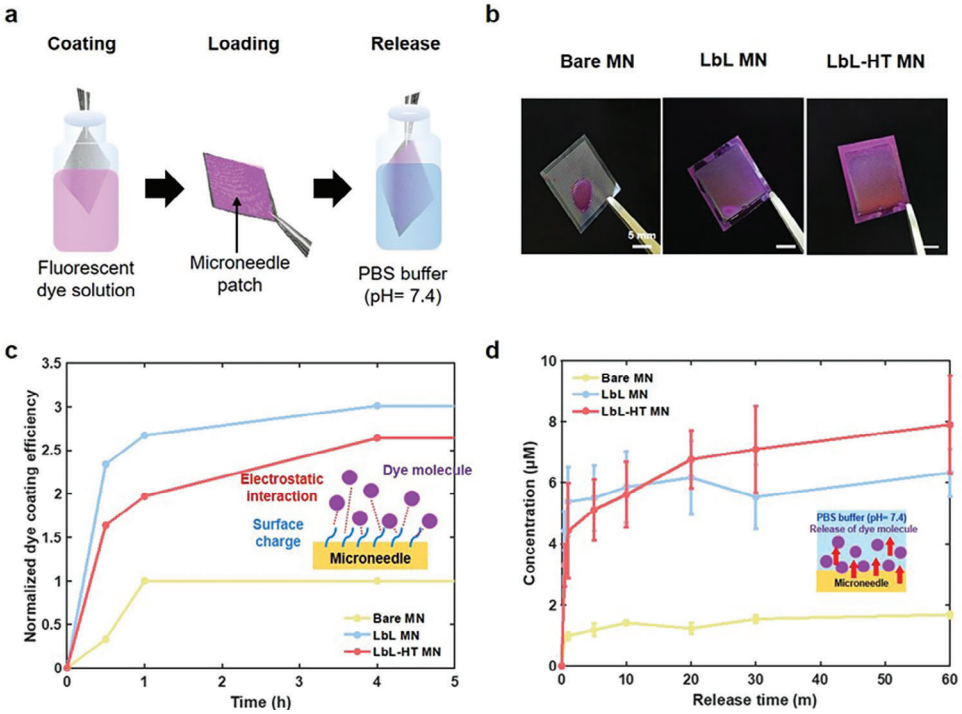

Figure 3. Drug coating and release tests of the MNs. a) Experimental setup of the drug coating and release test. (b) Images of the MNs after coating with sulforhodamine B (SRB) on bare, LbL, LbL-HT MN patches. Scale bars represent 5 mm. c) Dye coating capacity of the MNs using SRB. d) Graph showing the calibrated concentration of the released SRB in PBS (pH = 7.4).

with a weight of 300 g. We noted that the MNs did not break until we placed a weight of 200 g; this was considered a much harsher condition compared to the robustness test of other reports.[23] The fracture fraction was calculated to evaluate the mechanical durability of each sample. The fracture fraction is calculated as follows:

$$\text{Fracture fraction } (\%) = \frac{N_{\text{fracture}}}{N_{\text{total}}} \times 100 \quad (2)$$

where N_{fracture} is the number of fractured MNs, and N_{total} is the total number of the original MNs. We defined fracture as breakage at the base of the MNs. Figure 4c shows a SEM image of bare MNs after the mechanical test. The fracture fraction obtained from Figure 4c is 65%. On the other hand, the fracture fraction can be decreased to 10% after LbL (10 bilayers) -HT treatment as shown in Figure 4d. As shown in Figure 4e, the fracture fraction significantly decreased from 62.8% (bare MN arrays) to 22.4% (LbL MNs) as the thickness of the LbL film on the MNs increased. Moreover, the hydrothermal treatment further reduced the fracture fraction to 11.0% for the MNs with 10 bilayers. These results show that coating SiO_2 NPs on the MNs via the LbL assembly with higher thickness followed by hydrothermal treatment increased the mechanical robustness of the MNs.

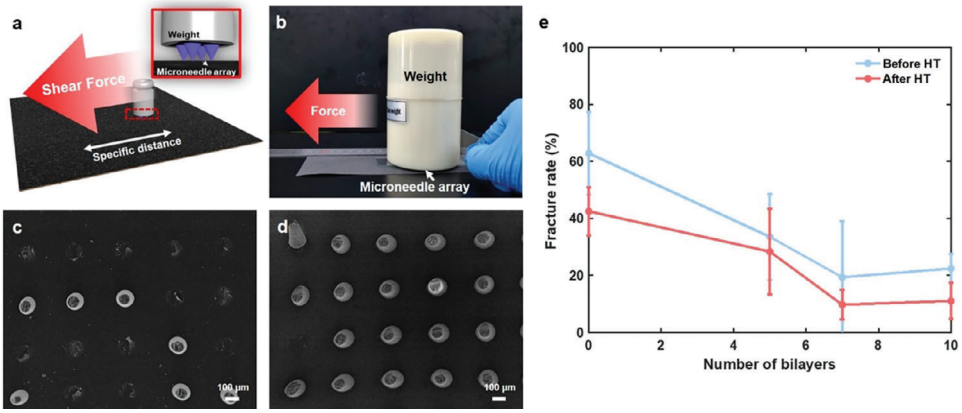

Figure 4. Mechanical tests of the MNs. a) Schematic and b) Image of experimental setup for the mechanical test. SEM images of c) bare MN arrays and d) LbL-HT MN arrays after mechanical test, e) fracture rate of the MNs with an increasing number of bilayers.

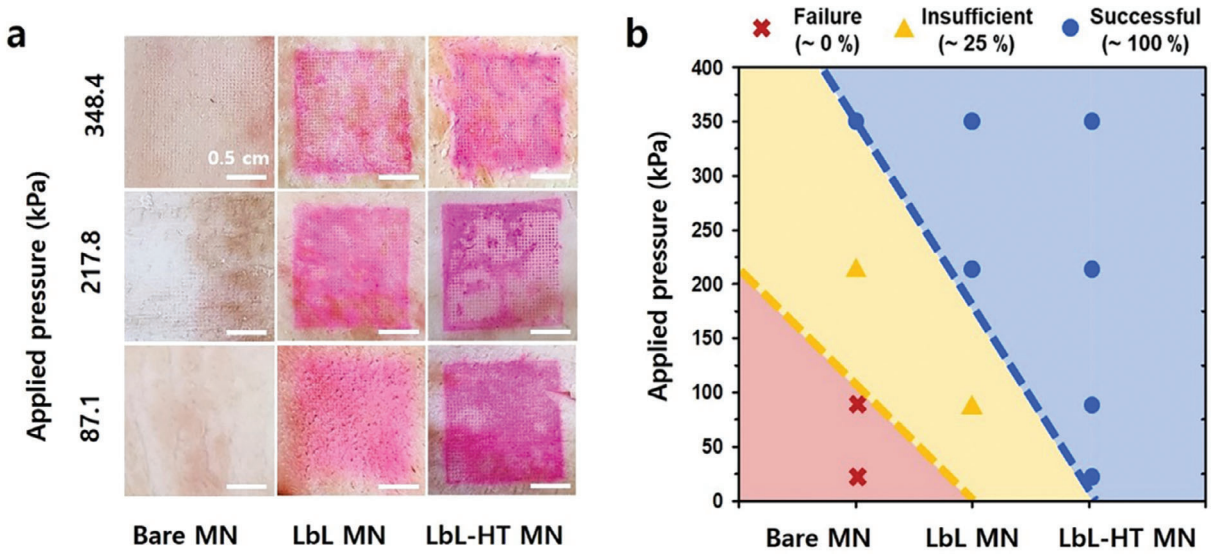

Figure 5. a) Images of the porcine skin after penetration according to the applied pressure. Scale bars represent 0.5 cm. b) Graph showing the result of penetration by the applied pressure.

A skin penetration test was performed using cadaver porcine skin, which has a similar hardness to human skin, using a load cell to maintain constant pressure. In a previous paper, we showed that PEGDA MNs could penetrate porcine skin without any fracture under pressures ranging from 435.6 to 958.2 kPa.[16] However, since MNs are applied to various areas of the body for different purposes, such as drug delivery or skin rejuvenation, a smallest possible pressure that induces penetration needs to be used to ensure the safety and comfort of the individual. Applying excessive pressure could potentially cause discomfort, skin damage, or even injury. Therefore, we evaluated the minimum pressure needed to penetrate porcine skin for each MN. **Figure** 5a shows the experimental setup of the penetration test. The sample was laid on porcine skin, and pressures of 21.8 kPa, 87.1 kPa, 217.8 kPa, and 348.4 kPa were applied. Figure 5b shows porcine skin after penetration with MNs under different conditions. When we applied a pressure of 87.11 kPa, the bare MNs could not penetrate the skin. However, the LbL MNs and the LbL-HT MNs could penetrate the skin. Figure 5c shows a graph indicating how each MN penetrated porcine skin by applying pressure. The bare MNs were not able to penetrate porcine skin under pressures of 21.8 and 87.1 kPa, but full penetration was attained when the pressure reached 348.4 kPa. The LbL MNs penetrated the skin under pressures of 21.8 and 87.1 kPa; however they had incomplete penetration, which could reduce the drug delivery efficiency. The LbL-HT MNs showed complete and successful penetration even under a pressure of 21.8 kPa. The MNs reinforced by SiO_2 NPs became stiffer and did not buckle during penetration, which could be the reason for the lower pressure threshold. We note that the LbL coating does not significantly affect the swelling of the MNs. The swelling ratio of MNs are less than 5% after dipping the sample in water bath for 24 h (Table S1, Supporting Information). The swelling ratio is smaller than other report because of the low MW (250 Da) of PEGDA prepolymer; the swelling ratio remains low when the MW of prepolymer is small.[24] Furthermore, the enhancement of mechanical robustness after LbL and LbL-HT shows that the swelling effect is negligible because we used the treated MNs after drying.

We also evaluated the penetrability of the MNs using a living rat model (**Figure 6**). Figure 6a shows a living rat after removing the dorsal skin by electric clippers and depilatory cream on the back. We applied the MN samples to the rat dorsal skin for 1 min. Figure 6b shows the histological image of the rat skin before applying MNs. We extracted the skin and stained it to observe the punctured tissue. As shown in Figure 6c,d, the LbL and LbL-HT MNs successfully penetrated the epidermal skin of living animal and reached the dermal tissue. Figure 6e shows a graph of cell viability test based on the standard of cytotoxicity (ISO 10993-5:2009).[25,26] After the elution of MN samples in water bath, the solution is treated on the human skin fibroblast cells in the assay. When the solution is diluted with water, the cell viability was 100%, which indicated negligible effect on cells. The viability was dropped to 77.8% when the solution is not diluted (100% in the x-axis), but it satisfied the standard of non-cytotoxicity (above 70% in the highest concentration).

3. Conclusion

Polymeric MNs are an ideal transdermal platform for diagnosis and treatment due to their processability and biocompatibility. However, they need high pressure for successful penetration due to the lack of stiffness. In this study, we engineered polymeric MNs with LbL thin films containing SiO_2 NPs for enhancing drug loading and mechanical strength. The LbL assembly enabled facile control of the physical properties without changing the MN geometry. Additionally, the film was hydrothermally treated to further enhance drug release and mechanical strength. The LbL thin film-coated MNs showed the highest drug coating, while hydrothermally treated LbL thin film-coated MNs showed the highest drug release, indicating high drug delivery efficiency. The LbL thin film-coated MNs showed high resistance to fracture during the mechanical test and successful penetration at

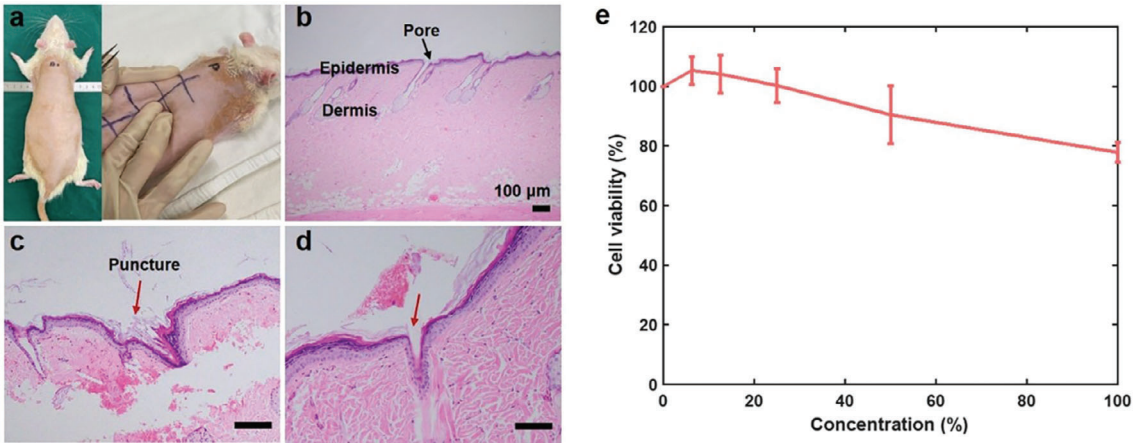

Figure 6. Evaluation of in vivo penetration test and in vitro cell viability. a) Image of a rat for historical tests. b) Image of the control rat skin. Images of rat dorsal skin punctured using c) LbL MNs and d) LbL-HT MNs. e) In vitro cytotoxicity evaluation of LbL-HT MNs.

relatively low pressures. The hydrothermally treated LbL thin film-coated MNs exhibited even higher resistance to fracture under the mechanical test than the other MNs and penetrated porcine and rat skin under the lowest pressure. The LbL assembly of SiO_2 NPs accompanied by hydrothermal calcination could be applied to many different types of polymer-based microdevices to improve their mechanical properties and thus enhance their functionality.

4. Experimental Section

Preparation of Materials: Poly(ethylene glycol) diacrylate (PEGDA, molecular weight: 250), photoinitiator (PI) 2,2-dimethoxy-2-phenyl acetophenone (Irgacure 651), poly(diallyldimethylammonium chloride) solution (PDADMAC, average molecular weight: 200 000–350 000), Ludox TM-50 (diameter 22 nm, 50 wt% suspension in water), sodium chloride (NaCl), sodium hydroxide (NaOH), fluorescein isothiocyanate (FITC), rhodamine B (RhB), methylene blue, methyl orange, and sulforhodamine B (SRB) were purchased from Sigma–Aldrich. Polydimethylsiloxane (PDMS) was purchased from Dow Corning (SYLGARD 184, with 10% curing agent).

Preparation of the Polymeric MNs: A PDMS chamber with inlet holes was prepared and covered with a polyethylene terephthalate (PET) film. The PET film (SKC, Korea) was used as a substrate for MNs produced by photopolymerization because of its thin thickness (50 μm) and high transmittance (>90%). The prepolymer (PEGDA + 5 wt% PI) was added into the PDMS chamber through the inlet hole. Thereafter, the sample was placed under a photomask and exposed to UV light using a Fusion Cure 360 (MINUTA Tech).[16] The uncured prepolymer was removed by washing with ethanol, and the remaining MNs were fully cured for 2 h. A Fusion Cure 360 (MINUTA Tech, Republic of Korea) UV curing device (5.0 mW cm^{-2}) was used to cure the prepolymer.

LbL Assembly and Hydrothermal Treatment of the PEGDA MNs: The LbL assembly was performed both manually and automatically. Automatic dipping was performed using an HMS Series programmable slide stainer (Carl Zeiss, Germany). Eight baths containing two species (PDADMAC and SiO_2 dispersed in water) were prepared for the washing steps, and six water baths were used for washing steps. Then, solutions of 0.01 M PADAMAC (4.042 g), 0.1 M NaCl (7.305 g NaCl in 496 mL DI water), and 10 mg mL^{-1} Ludox TM-50 (5 g in 500 mL DI water) were prepared.

The cycle time was 15 min for deposition and 2 min, 1 min, and 1 min for washing. The samples were treated with plasma (oxygen plasma for 10 s at 250 mTorr) to generate an initial charge on the surface. The baths were cleansed with detergent and cleaned with 1.0 M NaOH solution under sonication for an hour to remove any remaining organic matter. Hydrothermal treatment was performed using an autoclave (ETC Sterilization Systems, USA). The samples were placed in the autoclave and treated at 123 °C for an hour. Wafers for measuring film thicknesses were pretreated with oxygen plasma and fixed vertically during the process to remove watermarks.[17] Figure S1 (Supporting Information) shows the corresponding thickness of the layers by the number of the LbL depositions.

Characterization of SiO_2 NPs on the PEGDA MNs: To characterize the MN surface, scanning electron microscopy (SEM) images were obtained using a Quanta 600 FEG ESEM with an acceleration voltage of 5 kV and an EM-30 (COXEM, Republic of Korea) with an acceleration voltage of 10 kV. Energy-dispersive X-ray spectroscopy (EDS) analysis was performed using secondary electron mode at 10 nm from the surface to isolate the LbL film.

Mechanical Tests of the MNs: To evaluate the mechanical strength of the MNs, two different mechanical tests were performed. First, to assess the strength against shear force, an abrasion test using sandpaper was performed. An upside-down MN patch was placed on sandpaper, and 300 g of weight was placed on the MN patch samples. The MNs were pushed laterally with a weight to apply shear force on the MNs. The fracture rate was calculated by counting the broken MNs after applying shear force.

Penetration Tests of the MNs: To evaluate the penetrability of MNs, a porcine skin sheet, which was purchased from a local butcher shop, was used as a model skin. Rhodamine B was used as a drug model. The MNs were dip-coated in rhodamine B solution for an hour and then inserted into the skin for 1 min.

Drug Coating and Release Test of the MNs: Sulforhodamine B (SRB) was used as a coating-release model. The MN patches were dipped in the dye solution for an hour. SRB was used to calculate the drug loading capacity of each MN. Additionally, SRB was coated on the MNs for an hour, and the fluorescence intensity was measured using FlexStation III (Molecular Devices, CA, USA) to evaluate the drug release ability. Figure S2 (Supporting Information) shows the calibration curve from the concentration of dyes and their fluorescence intensities.

Characterization of the Films: The thickness of the thin film was measured using an alpha-SE ellipsometer (J.A. Woollam Inc.). The contact angles of water on the MNs were measured by a Biolin Scientific Attension goniometer. The surface roughness and morphology of the thin film were measured by atomic force microscopy (NX10, Park Systems, Republic of Korea)

Animal Tests: The animal tests were performed at the Asan Institute for Life Sciences, Asan Medical Center, following the appropriate guidelines and regulations set forth by the Institutional Animal Care and Use Committee (IACUC). The IACUC adheres to the Institute of Laboratory Animal Resources (ILAR) and Animal Research: Reporting of In Vivo Experiments (ARRIVE) guidelines established by The National Centre for the Replacement, Refinement and Reduction of Animals in Research (NC3Rs).

The allocation of animals was performed randomly, without considering any additional factors or variables. A single investigator conducted all animal experiments and collected the data. Three male SD rats (20 weeks old, 400–450 g; Ja Bio, Suwon, Republic of Korea) were used for the experiments. Throughout the experiments, the animals were housed under controlled conditions of constant temperature and humidity, with free access to water and food. Before applying the MNs, the animals were anesthetized using a combination of tiletamine/zolazepam (50 mg kg^{-1}, Zoletil; Virbac, Carros, France) and xylazine (10 mg kg^{-1}, Rumpun, Bayer Korea, Seoul, Republic of Korea). To ensure accurate results, the fur on the dorsal skin was completely removed using electric clippers and depilatory cream after the animals were anesthetized. After the MNs were tested on skin divided into 8 regions, histological analysis of the cross-section where the MNs were applied was performed on the harvested skin. The skin samples were fixed with 4% formaldehyde, and the animals were sacrificed after harvest. The fixed tissues were rinsed with distilled water to remove the fixative for approximately 2 h. The samples were dehydrated in graded ethanol, cleared in xylene using a tissue processor (Excelsior ES, Thermo Fisher Scientific, USA) and embedded in paraffin blocks sectionally using a paraffin embedding station (EG1150H, Leica, Germany). The paraffin blocks were cut into 4 µm thick sections on a rotary microtome (RM2255, Leica, Germany). The paraffin sections were stained with hematoxylin and eosin (H&E) to identify the shape of the skin puncture. This research was conducted using preclinical animal trials and did not incorporate materials derived from humans or involve human clinical trials. The Asan Institute for Life Sciences at Asan Medical Center's Institutional Animal Care and Use Committee (IACUC) granted approval for the number of animals used and oversaw all procedures involving animals in accordance with established protocols, including those set forth by the ILAR and ARRIVE guidelines (2022-12-110).

Cytotoxicity Tests: The cell viability test was conducted based on ISO 10993-5:2009. After the elution of MN samples at a concentration of 0.1 g mL^{-1} in 37° water bath for 24 h, the eluted water was filtered using a 0.45 µm pore size syringe filter. Human skin fibroblast cells (CCD-986sk) were used in the assay.

Supporting Information

Supporting Information is available from the Wiley Online Library or from the author.

Acknowledgements

S.K. and H.C. contributed equally to this work. H.Y. was supported by National Research Foundation of Korea (NRF) (grant numbers RS-2024-00341884 and NRF-2020R1A2C1011571). The authors also thank Prof. Junhyong Kim for the support of this work. K.S. and D.L. were supported by the National Science Foundation (1945841). H.J. and D.L. were supported by the National Human Genome Research Institute of the National Institutes of Health under Award Number RM1HG010023. The content is solely the responsibility of the authors and does not necessarily represent the official views of the National Institutes of Health.

Conflict of Interest

The authors declare no conflict of interest.

Data Availability Statement

The data that support the findings of this study are available from the corresponding author upon reasonable request.

Keywords

drug delivery, layer-by-layer, microneedle, nanoparticle, polymer

Received: March 23, 2024
Revised: June 2, 2024
Published online: June 22, 2024

[1] R. K. Mishra, K. Y. Goud, Z. Li, C. Moonla, M. A. Mohamed, F. Tehrani, H. Teymourian, J. Wang, *J. Am. Chem. Soc.* **2020**, *142*, 5991.
[2] J. Zhu, X. Zhou, H. J. Kim, M. Qu, X. Jiang, K. Lee, L. Ren, Q. Wu, C. Wang, X. Zhu, P. Tebon, S. Zhang, J. Lee, N. Ashammakhi, S. Ahadian, M. R. Dokmeci, Z. Gu, W. Sun, A. Khademhosseini, *Small* **2020**, *16*, 1905910.
[3] H. Chang, M. Zheng, S. W. T. Chew, C. Xu, *Adv. Mater. Technol.* **2020**, *5*, 1900552.
[4] L. Ventrelli, L. M. Strambini, G. Barillaro, *Adv. Healthcare Mater.* **2015**, *4*, 2606.
[5] K. Lee, M. J. Goudie, P. Tebon, W. Sun, Z. Luo, J. Lee, S. Zhang, K. Fetah, H.-J. Kim, Y. Xue, M. A. Darabi, S. Ahadian, E. Sarikhani, W. Ryu, Z. Gu, P. S. Weiss, M. R. Dokmeci, N. Ashammakhi, A. Khademhosseini, *Adv. Drug Delivery Rev.* **2020**, *165-166*, 41.
[6] X. Jiang, W. Xia, J. Pan, W. Yang, S. Zhang, C. Li, T. Zan, Y. Lai, Z. Xu, H. Yu, *Appl. Mater. Today* **2023**, *31*, 101774.
[7] A. vander Straeten, M. Sarmadi, J. L. Daristotle, M. Kanelli, L. H. Tostanoski, J. Collins, A. Pardeshi, J. Han, D. Varshney, B. Eshaghi, J. Garcia, T. A. Forster, G. Li, N. Menon, S. L. Pyon, L. Zhang, C. Jacob-Dolan, O. C. Powers, K. Hall, S. K. Alsaiari, M. Wolf, M. W. Tibbitt, R. Farra, D. H. Barouch, R. Langer, A. Jaklenec, *Nat. Biotechnol.* **2024**, *42*, 510.
[8] P. Bollella, S. Sharma, A. E. G. Cass, R. Antiochia, *Electroanalysis* **2019**, *31*, 374.
[9] F. Ribet, G. Stemme, N. Roxhed, *Biomed. Microdevices* **2018**, *20*, 101.
[10] S. R. Chinnadayyala, I. Park, S. Cho, *Microchim. Acta* **2018**, *185*, 250.
[11] O. Olatunji, D. B. Das, M. J. Garland, L. Belaid, R. F. Donnelly, *J. Pharm. Sci.* **2013**, *102*, 1209.
[12] S. P. Davis, B. J. Landis, Z. H. Adams, M. G. Allen, M. R. Prausnitz, *J. Biomech.* **2004**, *37*, 1155.
[13] Y. K. Demir, Z. Akan, O. Kerimoglu, *PLoS One* **2013**, *8*, e77289.
[14] T. Waghule, G. Singhvi, S. K. Dubey, M. M. Pandey, G. Gupta, M. Singh, K. Dua, *Biomed. Pharmacother.* **2019**, *109*, 1249.
[15] L. Barnum, J. Quint, H. Derakhshandeh, M. Samandari, F. Aghabaglou, A. Farzin, L. Abbasi, S. Bencherif, A. Memic, P. Mostafalu, A. Tamayol, *Adv. Healthcare Mater.* **2021**, *10*, 2001922.
[16] S. Kim, H. Lee, H. Choi, K.-Y. Yoo, H. Yoon, *RSC Adv.* **2022**, *12*, 9550.
[17] Z. Gemici, H. Shimomura, R. E. Cohen, M. F. Rubner, *Langmuir* **2008**, *24*, 2168.
[18] R. K. Iler, *The Chemistry of Silica: Solubility, Polymerization, Colloid and Surface Properties and Biochemistry of Silica*, Wiley, New York **1979**, p. *866*.
[19] J. W. Tester, M. Modell, *Thermodynamics and Its Applications*, Prentice Hall PTR, Upper Saddle River, NJ **1997**.
[20] D. Chandra, A. J. Crosby, *Adv. Mater.* **2011**, *30*, 3441.
[21] E. Um, Y.-K. Cho, J. Jeong, *ACS Appl. Mater. Interfaces* **2021**, *13*, 15837.
[22] A. Sadeqi, G. Kiaee, W. Zeng, H. Rezaei Nejad, S. Sonkusale, *Sci. Rep.* **2022**, *12*, 1853.
[23] J. Kim, Y. Ryu, C. H. Kim, S. G. Heo, K.-Y. Yoo, H. Yoon, *Adv. Funct. Mater.* **2021**, *31*, 2010053.
[24] A. Cavallo, M. Madaghiele, U. Masullo, M. G. Lionetto, A. Sannino, *J. Appl. Polym. Sci.* **2017**, *134*, https://doi.org/10.1002/app.44380.
[25] P. Thangaraju, S. B. Varthya, *Cham: Springer* **2022**, *163*.
[26] J. J. Jeong, D. W. Lee, S. Y. Song, Y. Park, J. H. Kim, J. I. Kim, H. G. Kim, K. T. Nam, W. J. Lee, K.-H. Nam, J. H. Lee, *PLoS One* **2019**, *14*, e0212583.